Bioorganic & Medicinal Chemistry 17 (2009) 13–24

Contents lists available at ScienceDirect

Bioorganic & Medicinal Chemistry

journal homepage: www.elsevier.com/locate/bmc

Molecular modelling studies, synthesis and biological activity of a series of novel bisnaphthalimides and their development as new DNA topoisomerase II inhibitors

Rosanna Filosa [a,*], Antonella Peduto [a,†], Simone Di Micco [a,†], Paolo de Caprariis [a], Michela Festa [a], Antonello Petrella [a], Giovanni Capranico [b], Giuseppe Bifulco [a,*]

[a] Department of Pharmaceutical Science, University of Salerno, via Ponte Don Melillo, variante 11C, 84084 Fisciano, Italy
[b] Department of Biochemistry G. Moruzzi, University of Bologna, via Irnerio 48, 40126 Bologna, Italy

ARTICLE INFO

Article history:
Received 28 October 2008
Accepted 11 November 2008
Available online 18 November 2008

Keywords:
Anticancer naphthalimides
DNA topoisomerase II inhibitors

ABSTRACT

A series of bisnaphthalimide derivatives were synthesized and evaluated for growth-inhibitory property against HT-29 human colon carcinoma. The *N*,*N*′-bis[2-(5-nitro-1,3-dioxo-2,3-dihydro-1H-benz[*de*]-isoquinolin-2-yl)]propane-2-ethanediamine (**9**) and the *N*,*N*′-Bis[2-(5-nitro-1,3-dioxo-2,3-dihydro-1H-benz[*de*]-isoquinolin-2-yl)]butylaminoethyl]-2-propanediamine (**12**) derivatives emerged as the most potent compounds of this series. Molecular modelling studies indicated that the high potency of **12**, the most cytotoxic compound of the whole series, could be due to larger number of intermolecular interactions and to the best position of the naphthalimido rings, which favours π–π stacking interactions with purine and pyrimidine bases in the DNA active site. Moreover, **12** was designed as a DNA topoisomerase II poison and biochemical studies showed its effect on human DNA topoisomerase II. We then selected the compounds with a significant cytotoxicity for apoptosis assay. Derivative **9** was able to induce significantly apoptosis (40%) at 0.1 μM concentration, and we demonstrated that the effect on apoptosis in HT-29 cells is mediated by caspases activation.

1. Introduction

Anticancer naphthalimides constitute an important class of drugs characterized by a high cytotoxic activity upon a variety of murine and human tumour cells.[1] These drugs perform their biological activity either by forming a DNA-intercalator-topoisomerase II (topo II) ternary complex or by inhibiting other enzymes and/or transcription factors that act on DNA. The strong interactions with DNA play a crucial role for their pharmacological properties. Significant examples include compounds such as monomeric naphthalimides (**1**: amonafide **2**: mitonafide) and bisnaphthalimides (**3**: LU 79553-elinafide, **4**: DMP 840-bisnafide).

Nowadays, it is accepted that the planar system of these drugs can intercalate the DNA base pairs. In the case of amonafide and mitonafide the antitumour activity is closely related to their ability to poison human DNA topo II. Moreover, bisnafide analogues kill eukaryotic cells by stabilizing the cleavage complex of topo II with

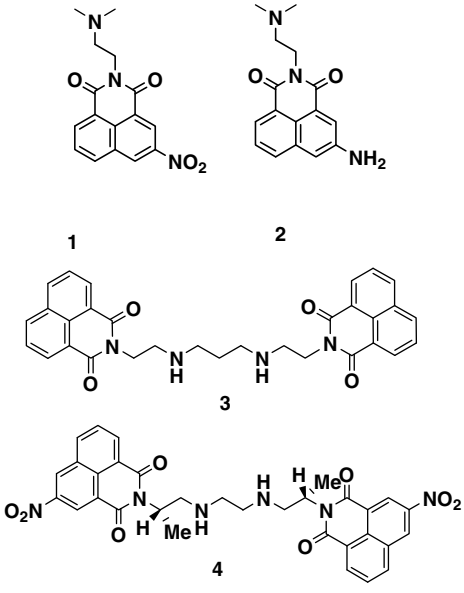

* Corresponding authors. Tel.: +39 089969749; fax: +39 089 962828 (R.F.), Tel.: +39 089969741 (G.B.).
E-mail addresses: rfilosa@unisa.it (R. Filosa), bifulco@unisa.it (G. Bifulco).
† Contributed equally to this work.

0968-0896/$ - see front matter © 2008 Elsevier Ltd. All rights reserved.
doi:10.1016/j.bmc.2008.11.024

Table 1
First series of bisnaphthalimides derivatives

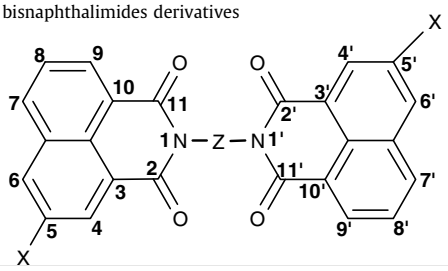

5: X= NO_2; Z=

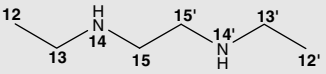

6: X= NO_2; Z=

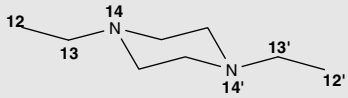

7: X= NO_2; Z=

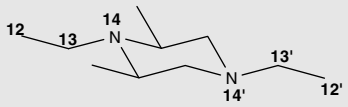

8: X= NO_2; Z=

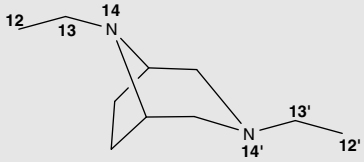

9: X= NO_2; Z=

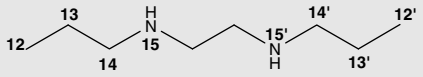

10: X= NO_2; Z=

DNA.[2] However, this is still controversial as previous studies have reported that elinafide is not a poison of topo II.[3–6]

Most of the research has been traditionally focused on the modification of the naphthalimido ring to enhance anticancer activities through increased DNA-binding and cleavage.[7]

In order to develop more active DNA-binding antitumour agents, and to clarify the influence of the aminoalkyl linker chain in their intricate modes of action, a novel series of bisnaphthalimides have been synthesised.

The first series (Table 1) were originally designed and synthesized as bisintercalating agent, starting from previous findings on the structural requirements for DNA-binding of **3** and **4**.

The synthesis of compounds **5–10** was accomplished by linking the two heteroaromatic moiety employing a variety of dicationic linker chains where the length, rigidity, and charge density on the chain are varied.

In order to gain new detailed molecular insights into their binding to DNA, we have studied the compounds **5–10** by docking calculations.

Following the docking results observed for **5**–**10**, we have focused our attention on designing new topo II inhibitors. We have rationalized, through virtual screening, the length and chemical structure of the aminoalkyl linker to improve the interactions with the biological target.[8]

2. Chemistry

Polyamines **14a–c** from which the bisnaphtalimides **6**, **7** and **8** were prepared and then were carried out following the method outlined in Scheme 1. Thus, the two nitrogens of heterocycles piperazine, *cis*-dimethylpiperazine, 3,8-diazabicyclo[3.2.1]octane (DBO)[9] were treated with chloroacetonitrile, in the presence of sodium carbonate, to yield the dinitriles **13a–c**. Reduction of these with lithium aluminium hydride led to the corresponding amines **14a–c**.

The synthesis of (±)-(*trans*)-N^1,N^2-bis(2-aminoethyl)cyclopropane-1,2-diamine **19** involved the cyclopropane-1,2-dicarboxylic acid **15** as the starting material[10] (Scheme 2). The conversion of dicarboxylic acid **15** to diamine moiety **16** was accomplished by a modified Curtius reaction involving the formation of carboxylic azides and a final treatment with aqueous HCl.[11] The diamine **16** was converted into the corresponding acylated derivative **17**, at each end, with Boc-β-alanine in the presence of carbonyldiimidazole (CDI). Treatment of **17** with HCl and subsequent borane reduction afforded in high yield the corresponding polyamine **19**.

The rest of amines triethylenetetramine and *N*,*N*′-bis(3-aminopropyl)-ethylenediamine used for synthesis of compounds **5** and **9** were commercially available.

The preparation of the corresponding bisnaphtalimides **5–10** was achieved following the synthetic protocol by reaction of 3-nitro-1,8-naphthalic anhydride with the corresponding polyamine (see Scheme 3).

3. Structure–activity relationships for cellular growth inhibition

3.1. Cytotoxicity

The in vitro cytotoxicity of all the bisnaphthalmido derivatives was studied in the human colon adenocarcinoma HT-29 cell line as described in methods section.

Compounds **5–10** were tested as methanosulfonate salts.

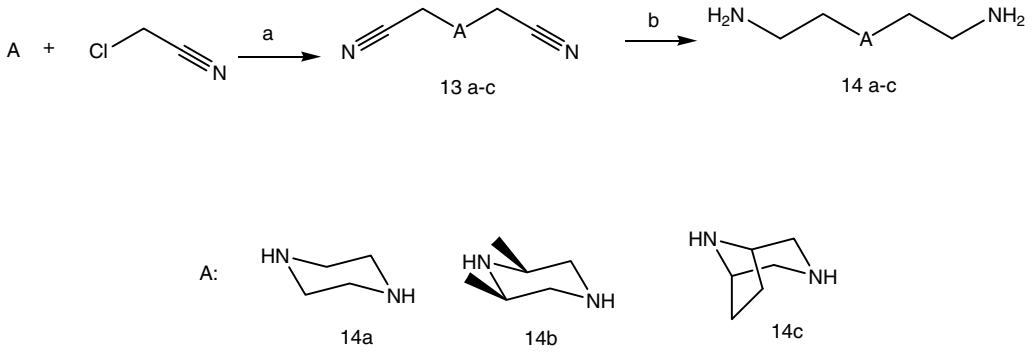

Scheme 1. Reagents and conditions: (a) Na_2CO_3/EtOH, 18 h, Δ; (b) $LiAlH_4$/THF, 4 h, Δ.

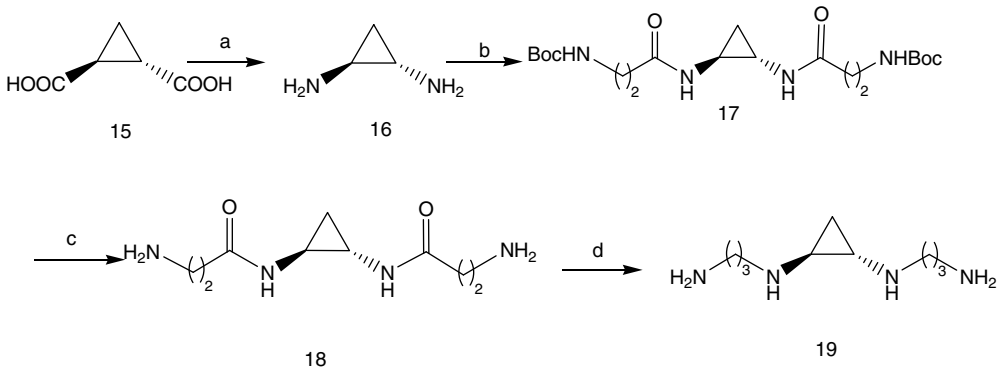

Scheme 2. Reagents and conditions: (a) i—$SOCl_2$, benzene, 60–70 °C, 24 h; ii—NaN_3/H_2O, acetone, 0 °C, 2 h; iii—toluene Δ, 6 h; iv—HCl concd, EtOH 95%, Δ, 5 h; (b) N-Boc-β-alanine, CDI/CH_2Cl_2 0 °C-rt, 18 h; (c) HCl gas, MeOH, 1 h, 0 °C, 18 h rt; (d) BH_3–THF/THF, Δ, 24 h.

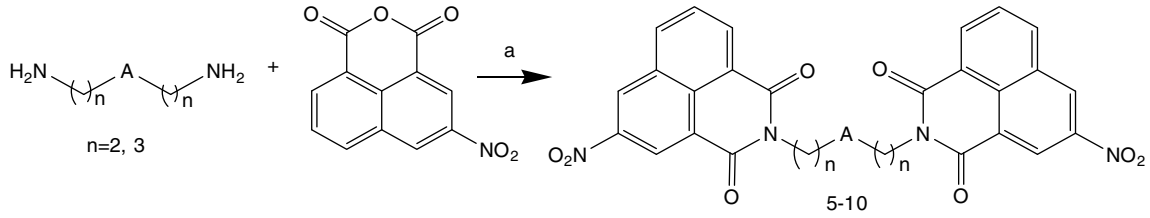

Scheme 3. Reagents and conditions: toluene/EtOH, 4 h, Δ.

Table 2
Cytotoxic potency of mono- and bisnaphthalimides **5**–**10** in the human HT-29 cell line

Compound	IC_{50}[a] HT-29
5	0.200
6	2.1
7	6.1
8	7.3
9	0.501
10	3.3
Elinafide	0.038

[a] IC_{50}: the drug concentration (μM) that reduces the cell number of treated samples to 50% of control cultures.

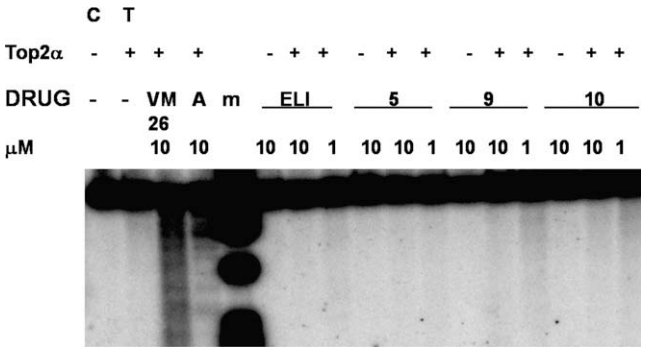

Figure 1. DNA cleavage stimulated by bisnaphthalimides **5**, **9** and **10**. Symbols are as follows: C, control DNA; T, topo IIα only; m, molecular DNA markers; VM-26, teniposide; A, Amonafide; ELI, elinafide. Compounds were tested at the indicated doses with or without topo IIα.

The activity of the cytotoxic drugs and IC_{50} values were determined after 72 h of drug exposures (Table 2). The IC_{50} values of the tested compounds range from 0.04 to 6.1 μM.

Thus, the compounds containing a linear carbon chain (**5** and **9**) were more potent than the constrained analogues (**6**, **7**, **8** and **10**). Compound **5** was the most active derivative, in which a linear aminoalkyl linker with two methylene groups separate chromophores from the central ethylendiamine.

The removal of flexibility from the linker chain by incorporating a piperazine, *cis*-dimethylpiperazine or DBO (**6**, **7** and **8**) determined a decrease of cytotoxicity.

On the contrary compound **9**, with the longer linker chain separation distance (11.0 Å) showed a good activity at nanomolar range concentration in HT-29 cells.

When the central ethylendiamine was replaced by a cyclopropane, (**10**) the cytotoxic activity decreased.

3.2. Mechanism of action studies

3.2.1. Topoisomerase inhibition

With respect to the molecular activity the first investigation dealt with the ability to interfere with DNA functions.

We analysed the possibility that this class of compounds could poison topo II. The relative drug activity in stimulating topo II-mediated DNA cleavage was studied using the pBR322 DNA as a substrate for the recombinant human DNA topo IIα.

The data in Figure 1 show that derivates **5**, **9** and **10** were ineffective in stimulating DNA cleavage, even though **9** and **10** somewhat showed a slight smear more evident than elinafide, that may correspond to cleaved DNA fragments at the lowest tested dose (1 μM). It is well known that topo II poisons with a strong DNA-binding activity repress topo II-mediated DNA cleavage at high concentrations in vitro and in vivo.[12]

The findings thus show that the tested compounds are marginally active as topo II poisons, suggesting a different mechanism of action.

3.2.2. Cell cycle effects

To investigate the effects of these compounds in more detail, we examined the activity on proliferation and cell cycle progression in HT-29 cells.

The analysed compounds are not able to block cell cycle progression of HT-29 cells (data not shown).

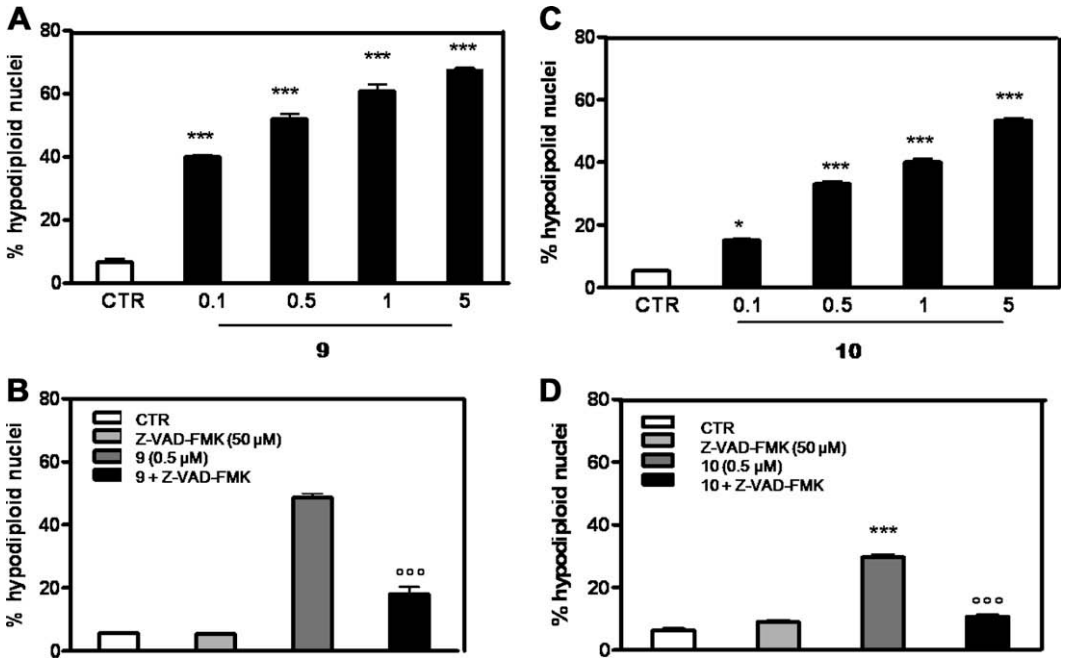

Figure 2. Apoptosis detection by propidium iodide (PI) staining of hypodiploid nuclei. HT-29 cells were incubated with **9** and **10** compounds (0.1–5 mM) for 48 h. Treatments of **9** at 0.1 μM (A) and **10** at 0.5 μM (C) induce a significant apoptosis off HT-29 cells ($^{***}P < 0.001$ vs CTR). To study involvement of caspases in **9** and **10** induced apoptosis a general caspases inhibitor (Z-VAD-FMK) was administrated 30 min before both compounds. Z-VAD-FMK (50 μM) inhibits effect of **9** (B, $^{\circ\circ\circ}P < 001$ vs 9) and **10** (D, $^{\circ\circ\circ}P < 0.001$) on apoptosis of HT-29 cells. Data shown are representative of three experiments performed in triplicate.

3.2.3. Pro-apoptotic effects of compounds 9 and 10 on human colon carcinoma cells

In order to understand the mechanism involved in cellular death, compounds **5–10** were tested as pro-apoptotic agents. Among all compounds analysed, compounds **9** and **10** showed pro-apoptotic effects. We have checked the activity of compounds on apoptosis using propidium iodide staining by flow cytometry as described in methods section. HT-29 cells were incubated with compounds **9** and **10** at different concentrations (0.1–5 μM) for 48 h. Results in Figure 2 showed a significant increase in apoptotic cells after treatment with **9** (Fig. 2A) and **10** (Fig. 2C). These effects are dependent to concentration used and the compound **9** was more able to induce a significant apoptosis (40%) at 0.1 μM concentration. In addition we demonstrated that pro-apoptotic effects of **9** was mediated by caspases activation. Cells were treated with general caspases inhibitor Z-VAD-FMK (50 μM) for 30 min before **9** (Fig. 2B) and **10** (Fig. 2D). Z-VAD-FMK inhibits significantly the pro-apoptotic effects of both compounds to demonstrate involvement of caspases in their apoptotic effect.

3.2.4. DNA-binding properties

With the aim to explore the structural determinants responsible for the activity of this new series of bisnaphthalimides, a molecular modelling study has been carried out for **5**–**10**.

Docking studies were performed on **5–10** with two DNA models (Fig. 3, Models A and B), using AutoDock 3.0.5 software.[13]

The Model A was derived by the NMR solution complex between the duplex d(CGCTAGGCG)-(GCGATCCGC) and the bis-thiazole orange, and the Model B was built from Model A (see experimental section for details) substituting two central base pairs.

Both models were used to evaluate the influence of the base sequence on the binding affinity.

DNA intercalators, like **3**, are reported to show a GC sequence preference[2] and, as it will be shown below, our docking results are in agreement (Table 3).

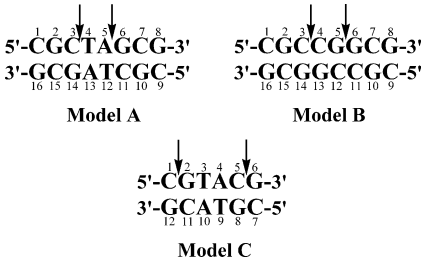

Figure 3. Schematic representation of DNA Models (A, B and C) used in the docking calculations. Sequence and numbering of two 8mers (A and B) and 6mer (C) DNA duplexes are reported. The arrows indicate the intercalation points.

For sake of simplicity we will describe in this section only the detailed docking results obtained with Model B.

The partial charges of the ligands (**3** and **5**–**10**) were calculated at DFT B3LYP level and 6-31G+(d) basis set using the ChelpG[14] method for population analysis and were used in the subsequent docking calculations.

In the theoretical studies, we considered the amine functionality as protonated at physiological pH and, consequently, positively charged in the calculations.

Table 3
Values of calculated inhibition constant[a] associated with the complex between **5–10** and Models A and B

Compound	K_i	
	Model A	Model B
3	1.51×10^{-14}	2.39×10^{-15}
5	1.99×10^{-13}	6.62×10^{-14}
6	3.37×10^{-12}	7.75×10^{-13}
7	2.24×10^{-14}	8.83×10^{-15}
8	3×10^{-14}	6.57×10^{-15}
9	9.09×10^{-15}	3.45×10^{-15}
10	5.35×10^{-15}	1.03×10^{-15}

[a] The inhibition constant is expressed as M and it is calculated at 293.15 K.

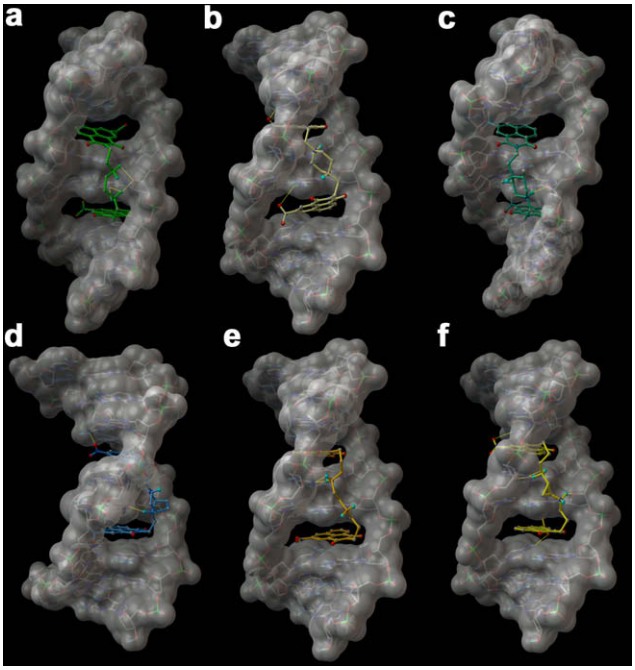

Figure 4. 3D models of the interactions between **5–10** (respectively, a, b, c, d, e and f) and the Model B. The DNA is represented by molecular surface and tube (coloured by atom type: C, grey; polar H, sky blue; N, dark blue; O, red). All ligands are depicted by sticks (green for **5**, light yellow for **6**, esmerald for **7**, blue for **8**, orange for **9** and yellow for **10**) and balls (by atom type). The figure highlights essential interactions: the naphthalimides are intercalated between base pairs and the linker interacts with the minor groove. The amino groups establishe hydrogen bonds (indicated by yellow lines) with nucleotides in the minor groove.

The analysis of docking results reveals that all ligands share a similar binding mode (Fig. 4). In details, the common structural portion, constituted by a polycyclic system, is fundamental for the line up of the complex with the biological target, through a base pairs intercalation. The linker of two naphthalimides also plays a crucial role in the affinity to nucleic acids, contributing to the complex stability interacting with the minor groove of the DNA.

The structure **5** establishes π–π interactions with DNA aromatic rings, through intercalated naphthalimides (Fig. 4a) and these interactions are extended thanks to the presence of the nitro groups on the aromatic portions. The linker chain establishes Van der Waals contacts and hydrogen bonds with nucleic acids. In particular, both amino groups interact with the anomeric oxygen of deoxyribose and N3 of G5, whereas the NH_2 14′ forms a further hydrogen bond with N3 of the same residue (Fig. 4).

Same considerations were applied for structures **6**–**8**. The planar moiety forms Van der Waals interactions with DNA base pairs, and the nitro groups are involved in further intermolecular interactions (Fig. 4b, c and d).

In particular, for **6**, the nitro functionality in 5 makes an hydrogen bond with NH_2 in 4 of a C3, whereas the other nitro group is hydrogen bonded to the NH_2 in **2** of G5 (Fig. 4b).

The linker chain results collocated into the minor groove, with the piperazine ring arranged in a parallel fashion with respect to the deoxyribose groove walls of the DNA, providing hydrophobic contacts. Moreover, in compound **6**, the linker amine groups are not involved in hydrogen bonds, causing a lower predicted binding affinity compared to **5** (Fig. 4b). Same considerations were applied for structures **6**–**8**. The planar moiety forms Van der Waals interactions with DNA base pairs, and the nitro groups are involved in further intermolecular interactions (Fig. 4b, c and d). In particular, for **6**, the nitro functionality in 5 makes an hydrogen bond with NH_2 in 4 of a C3, whereas the other nitro group is hydrogen bonded to the NH_2 in **2** of G5 (Fig. 4b).

The linker chain results collocated into the minor groove, with the piperazine ring arranged in a parallel fashion with respect to the deoxyribose groove walls of the DNA, providing hydrophobic contacts. Moreover, in compound **6**, the linker amine groups are not involved in hydrogen bonds, causing a lower predicted binding affinity compared to **5** (Fig. 4b). For compound **7**, as observed for **5**, nitro functionalities do not establish hydrogen bonds; on the other hand, NH^+ 14′ of piperazine makes an hydrogen bond with the N3 and anomeric oxygen of deoxyribose of G5 (Fig. 4c), while the remaining amino group points outside the minor groove. The dimethyl piperazine ring shows extended hydrophobic contacts, facing the purine/pyrimidine bases of the minor groove (Fig. 4c). While the nitro group in 5 of compound **8** presents the same interaction observed for **6** (Fig. 4d), the NH^+ 14′ of piperazine is hydrogen bonded to the N3 of guanine 5, as found for **7**. NH^+ 14′ also faces the external aqueous environment, as observed in **7**. Moreover the 3,8-diazabicyclo[3.2.1]octane gives more extensive Van der Waals interactions with its macromolecular counterpart.

While the linker length is maintained comparable, the structural difference between **5** and **6**–**8** is characterized by a linker tightening due to the insertion of a piperazine ring in the central part of the chain. Such bulky moiety, especially for **7** and **8**, contributes to complex stability through several Van der Waals interactions with the minor groove. In fact, the compounds **7** and **8** show a better binding affinity for the biological target with respect to **5** (Table 3).

Structure **9** establishes two hydrogen bonds by amino group 15 with the N3 of G13 (Fig. 4e). Compound **9** is similar to **5**, but it has a longer aminoalkyl linker length: 13.8 Å versus 11.1 Å of structure **5** (Fig. 5a).

In **9** there are three methylenes between the polycyclic moiety and the nitrogen of the linker. This longer chain influences the binding affinity to the DNA, because it allows a better intercalation of both aromatic systems compared to the preceding compounds (Fig. 5a).

In details, both planar portions of the ligand can make more effective π–π interactions with DNA base pairs, and the aminoalkyl chain establishes closer Van der Waals contacts and hydrogen bonds with the minor groove of the nucleic acid.

Similar results are found for **10**, because it presents approximately the same aminoalkyl chain length (13.5 Å) of **9** (Fig. 5b). As reported in Figure 5b, **9** and **10** showed an overlapped binding mode, with cyclopropane superimposed to central ethylenes of the aminoalkyl linker of **9**. Compound **10** establishes by NH_2^+ 15 the same interactions found for **9**, and a further hydrogen bonds with the anomeric oxygen of deoxyribose of G13 (Fig. 4f). The NH_2^+ 15′ only interacts with anomeric oxygen of deoxyribose of G5 residue. Both nitro groups, differently from **9**, are involved in hydrogen bonds.

In details, the nitro groups 5 and 5′ interact with NH_2 in 4 of C3 and C11, respectively (Fig. 4f). Moreover, the cyclopropane ring faces the individual base pairs along the groove floor, contributing by Van der Waals contacts to the complex stability.

Thus **10** exerts, compared to **9**, a slightly more efficient binding affinity (Table 3) for the biological target thanks to a larger number of intermolecular interactions. We have also performed docking calculations on elinafide (**3**) as reference structure. Comparing **3** with **10**, we observed a similar binding mode. The NH_2^+ 15 encounters the same interactions found for **10**, whereas the remaining amino group 15′ is hydrogen bonded to the N3 of G5 residue. In the structure of elinafide the nitro functionalities and cyclopropane are not present and can not contribute by their interactions to the binding affinity improvement, causing a lower K_i value for **3**.

The theoretical outcomes, obtained docking the ligands on Model A, are in agreement with data collected with Model B. We

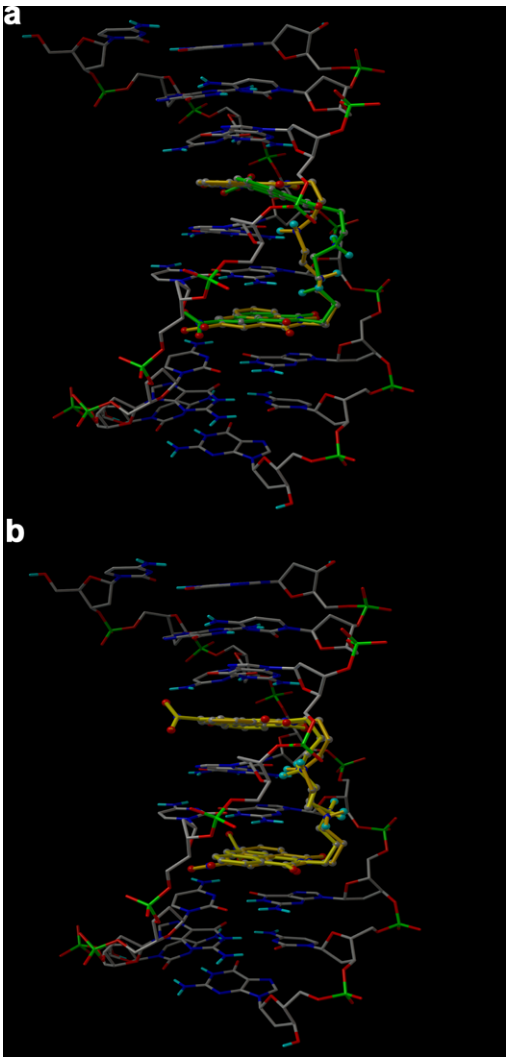

Figure 5. Compounds **5** and **9** (a), **9** and **10** (b), superimpositions in the DNA-binding site. The figure shows the influence of linker length on the contemporary intercalation of chromophore moieties. The DNA is represented by tube (coloured by atom type: C, grey; polar H, sky blue; N, dark blue; O, red). All ligands are depicted by sticks (green for **5**, orange for **9** and yellow for **10**) and balls (by atom type).

observed, in fact, a similar trend for ligands binding affinity. Moreover the comparison of docking results collected from Models A and B, shows a GC sequence preference in accordance with data reported in literature.[2] We observed for **5**–**10** docking poses on Model B the amidic CO group of chromophore moiety facing the NH_2 in 2 of guanine residue. This spatial arrangement extends the π–π interactions and probably gives raise to the little preference for GC sequences.

The predicted K_i are not perfectly in line with IC_{50} values describing the growth-inhibitory properties (Table 2). This is probably due to the possibility that each compound could interfere with more than a single biological process.

3.2.5. Design of novel topoisomerase II inhibitors

A crystal structure of a covalent topo II–DNA complex has not been solved, thus we have used a simplified model of the biological target in our docking calculations (Fig. 3, Model C).

It consists in a DNA duplex built from the X-ray structural complex between the double strand d(CG(Br-U)ACG)-(GCATCG) and two *N*-(2-(dimethylamino)ethyl)acridine-4-carboxamide. The choice of this experimental structure is dictated from the reaction mechanism catalysed by this protein. The topo II makes two breaks on both DNA strands with a four base pairs overhang and the enzyme becomes covalently linked to the 5′ ends of the break sites.[8] This transient covalent complex is the target of different drugs, that stabilize the ternary complex through a base pairs intercalation mechanism. As the choosen X-ray structural complex presents the intercalation points separated by 4 base pairs, it is consistent with our purpose to design topo II poisons.

The partial charges of the ligands are calculated by the same theoretical level employed for **5**–**10** and are used in the docking calculations.

Initially we have docked structure **3** as starting point for the development of new drugs. The docking pose of **3** shows only one chromophore portion intercalated between the DNA base pairs, because the aminoalkyl linker does not cover a 4 base pairs length. This finding has suggested us to lengthen the chain separating the two chromophore portions. We have tried various aminoalkyl linker (Table 4), and selected the structure **11**.

The aminoalkyl chain of **11** differs from the other elongated linkers for the number of amino groups. We have inserted two further amino functionalities to favour the hydrogen bonds formations with nucleotides. The central amino groups are separated by three carbon atoms as in **3**. The choice of the amino functionalities 16 and 16′ position along the chain, instead, is based on the distance between two consecutive base pairs. The theoretical studies showed that the linker length permitted the contemporary intercalation of both aromatic moieties of **11** and all amino groups are involved in hydrogen bonds with their macromolecular counterparts, gaining a better binding affinity ($K_i = 5.22 \times 10^{-18}$). The aminoalkyl chain perfectly collocates in the minor groove. It follows the helical turn covering the 4 base pairs distance and establishes significant hydrophobic contacts (Fig. 6a).

The NH_2^+ 16 and 16′ interact with O(=C) in 2 of C11 and C5, respectively, whereas the functionality 19 with N3 of A4. The amino group 19′ establishes hydrogen bonds with carbonilyc oxygen of T9, N3 of A10 and NH_2 of G8.

The analysis of docking studies on **5–10** has showed the nitro groups contribution to the complex stability by their interactions with purine/pyrimidine bases. Thus we have designed structure **12** with the common polycycle system of **5–10**.

The aminoalkyl chain is involved in hydrogen bonds. The NH_2^+ 16 and 19 are hydrogen bonded to anomeric oxygen of deoxyribose and N3 of A4 residue, and the NH_2^+ 16 makes further interactions with NH_2 of G2 and O(=C) of T3 (Fig. 6b).

The amino functionalities 19′ and 16′ establish hydrogen bonds with anomeric oxygen of deoxyribose of C5 and A10 residues. Moreover the NH_2^+ 16′ makes an hydrogen bond with O(=C) of T9 and with NH_2 of G8. The nitro groups extend π–π interactions with DNA base pairs, giving a slightly improvement of binding affinity ($K_i = 4.32 \times 10^{-18}$). Compared to **5–10**, compound **12** established more Van der Waals contacts and hydrogen bonds by its longer linker chain reaching a better complex stability. The experimental trials of growth-inhibitory properties, in fact, shows for **12** the most interesting IC_{50} value, in accordance with the theoretical data (Table 5). Moreover the theoretical outcomes are in agreement with the biological assays evaluating the Topoisomerase II inhibition. Compounds **5**, **9** and **10** do not inhibit the enzyme, whereas **12** shows an inhibition of the activity (see Scheme 4).

3.2.6. Chemistry

In order to synthesize compounds **11** and **12** in which more heteroatoms in the linker chain were introduced, N-alkylation reaction was chosen according to a modified method which was recently reported.[15]

The common intermediate for the synthesis of two derivatives is N^1,N^3,N^7,N^{10}-tetramesytil-1,3-bis(2-aminoethyl)-1,3-propanedi-

Table 4
Second series of bisnaphthalimides derivatives

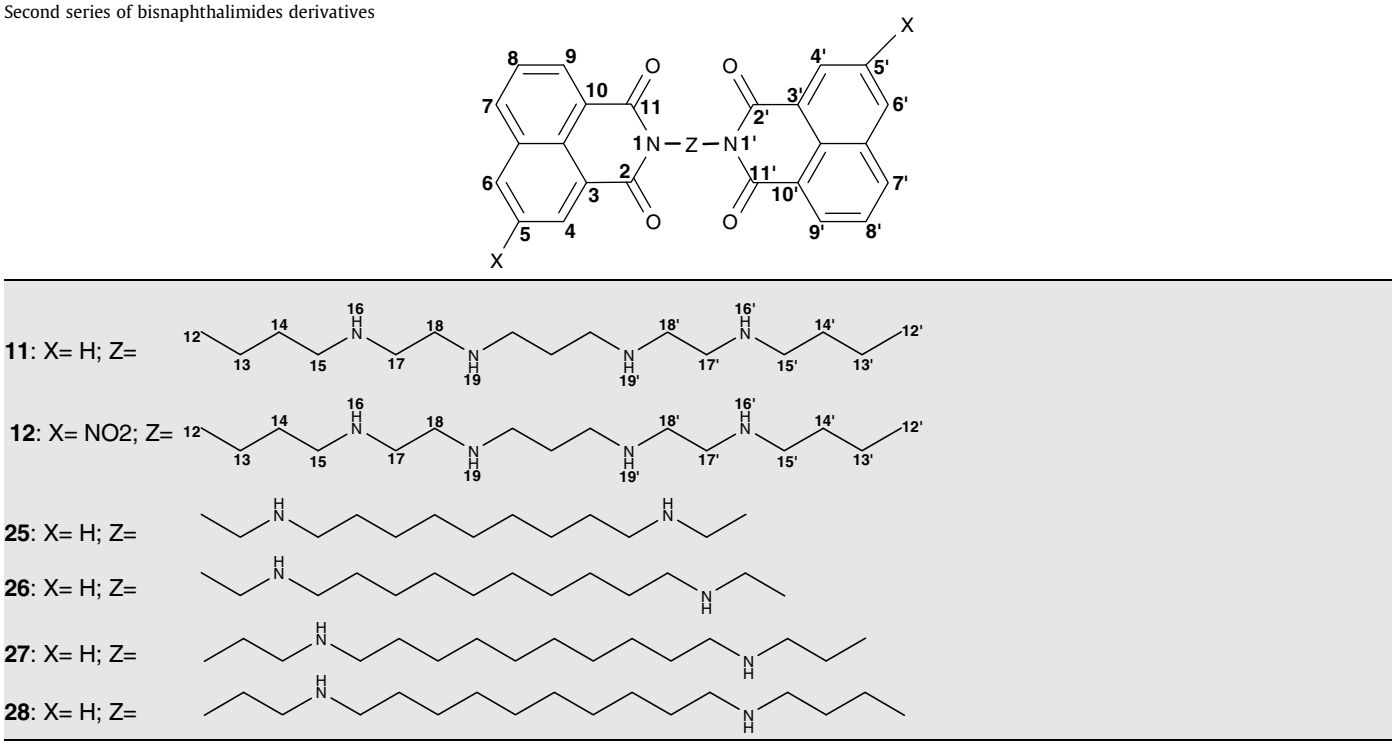

Table 5
Growth-inhibitory properties for Bisnaphthalimides **11** and **12** compared to elinafide and compound **5**

Compound	IC_{50}[a] HT-29
5	0.200
11	6.1
12	0.160
Elinafide	0.038

[a] IC_{50}: concentration of drug (μM) to reduce cell number to 50% of control cultures.

amine **23**. This was prepared reacting tetramine with mesitylene chloride in pyridine at room temperature. N-alkylation of the latter compound with *O*-tosylbutylnaphthalimides **22a–b**, with caesium carbonate in anhydrous DMF afforded the fully protected bis-naphthalimidobutyl derivatives **24a–b** which upon deprotection with hydrobromic acid/glacial acetic acid in dichloromethane afforded compounds **11** and **12**. *O*-Tosylbutylnaphthalimides **22a–b** were prepared by first reacting 1,8-naphthalic anhydride with aminobutanol to give *N*-(4-hydroxybutyl)naphthalimides **21a–b** which upon reaction with tosyl chloride gave **22a–b**. It is important to note that during the tosylation reaction, the best condition to obtain a maximum yield is to use four times excess of tosyl chloride in a small volume of solvent.[16] Under other conditions (e.g., with equimolar or 2 molar quantities of tosyl chloride), a mixture of *O*-tosylbutylnaphthalimide and *N*-(4-chlorobutyl)naphthalimide derivatives is always formed thus reducing the overall yield of the reaction and also, renders purification very difficult.

Among the latter compounds, derivative **12** showed the highest cytotoxicity against HT-29 cells with a IC_{50} value of 0.16 μM. The compound **11**, in which the nitro group was removed, was also cytotoxic but significantly less. Then, compound **12** was selected for the DNA cleavage assay in the presence of recombinant human topo IIα. The results reported in Figure 7 show that **12** is a topo II poison with a potency intermediate between amonafide and elinafide. **12** stimulated topo II-mediated breakage of pBR322 DNA at 10 μM (Fig. 7). Thus, our findings indicate that further structural modifications of the bisnaphthalimides series may lead to more effective inhibition of human Top2α.

4. Conclusion

The biological activity of naphthalimides is likely based on strong interactions with DNA in the target cells. Thus, we have here performed docking studies to rationalize the binding mode to nucleic acid evaluating the structural determinants of the binding affinities to the biological target. The analysis of docking results on **5**–**10** indicates all ligands as bis intercalating agents. The common planar moieties of the ligands intercalate between base pairs establishing π–π interactions with DNA aromatic rings, with nitro groups extending these intermolecular interactions or forming hydrogen bonds with nucleotides. The linker of two chromophores also contributes to complex stability because it can form, along the minor groove of the DNA, hydrogen bonds and Van der Waals contacts (especially where rings are present as structural elements of the linker chain).

The theoretical outcomes highlight that the linker chain length plays a crucial role in the binding affinity to DNA. Increasing the distance between two naphthalimides (in the series **5**–**10**), we reached more effective π–π interactions with base pairs and closer Van der Waals contacts and hydrogen bonds with the minor groove.

The docking results, obtained from **5**–**10**, have been the starting points to design new topo II poisons. Based on topoisomerase II catalysed mechanism, by a virtual screening we have designed the length and chemical structure (**11** and **12**) of the aminoalkyl linker to improve the interactions with the biological target.

The docking results suggest that to stabilize the ternary complex topo II–DNA-drug through a bisintercalator, it is fundamental a linker chain covering the four base pairs overhang. Such linker length causes a double intercalation in a position adjacent to the protein–DNA covalent bond.

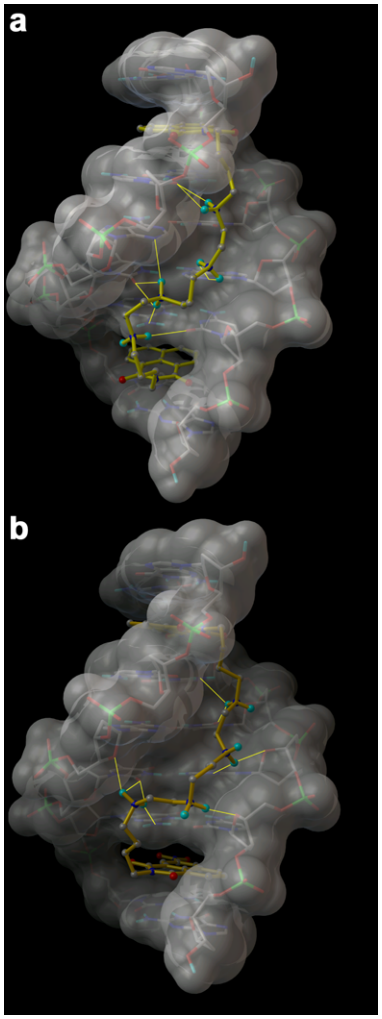

Figure 6. 3D models of the interactions between **11–12** (a and b, respectively) and the Model C. The DNA is represented by molecular surface and tube (coloured by atom type: C, grey; polar H, sky blue; N, dark blue; O, red). Two ligands are depicted by sticks (yellow for **11**, orange for **12**) and balls (by atom type). The figure highlights essential interactions: the naphthalimides are intercalated between base pairs and the linker interacts with the minor groove and allow a good bis intercalation. The amino groups establish hydrogen bonds (indicated by yellow lines) with nucleotides in the minor groove.

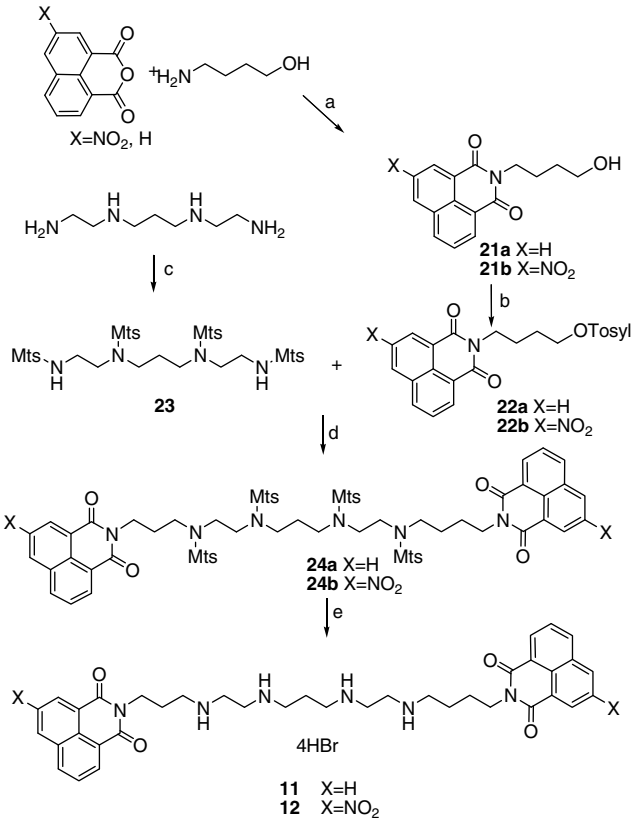

Scheme 4. Reagents and conditions: (a) H_2O, Δ, 40 °C; (b) tosyl-Cl, Et_3N/CH_2Cl_2, Δ, overnight; (c) Mts-Cl, Pyr, rt, 4 h; (d) $CsCO_3$/DMF, 80 °C, 18 h; (e) HBr/g·CH_3COOH, CH_2Cl_2, rt, 12 h.

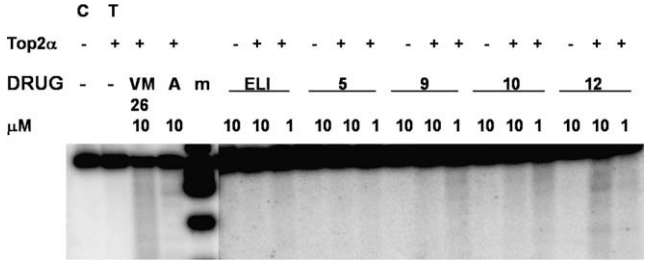

Figure 7. DNA cleavage stimulated by bisnaphthalimides **5**, **9**, **10** and **12**. Symbols are as follows: C, control DNA; T, topoisomerase IIα only; m, molecular DNA markers; VM-26, teniposide; A, amonafide; ELI, elinafide. Compounds were tested at 1 μM and 10 μM with or without enzyme.

The guidelines used to design new topo II poisons have been corroborated by biological assays. In details, compounds **5**, **9** and **10** do not inhibit the enzyme, whereas compound **12** shows a topo II inhibition. Moreover, the described agreement between theoretical and experimental data validates the reliability of our simplified model used to project new topo II poisons.

To design new anticancer compounds bisintercalating the DNA, the theoretical studies should suggest the use of a chromophore linker with suitable length to guarantee an optimum double intercalation between base pairs. The introductions of amino functionalities along the aliphatic chain and of donor/acceptor groups of hydrogen bonds on the planar portions, should also contribute to the binding affinity through a network of hydrogen bonds with the nucleotides.

5. Experimental

5.1. Chemistry

All reagents were analytical grade and purchased from Sigma–Aldrich (Milano, Italy). Flash chromatography was performed on Carlo Erba silica gel 60 (230–400 mesh; CarloErba, Milan, Italy). TLC was carried out using plates coated with silica gel 60F 254 nm purchased from Merck (Darmstadt, Germany). ^1H and ^{13}C NMR spectra were registered on a Brucker AC 300. Chemical shifts are reported in ppm. The abbreviations used are follows: s, singlet; d, doublet; dd double doublet; bs, broad signal. MS spectrometry analysis ESI-MS was carried out on a Finnigan LCQ Deca *ion trap* instrument. Elemental analysis was performed by Desert Analytics (Tucson, AZ).

5.2. General procedure for synthesis of 13a–c

To a solution of piperazine, 2,6-*cis*-dimethylpiperazine or DBO (1 g) and chloroacetonitrile (2.4 equiv) in absolute ethanol (50 mL), anhydrous sodium carbonate was added (4 equiv).

The reaction mixture was stirred at reflux for 4 h. The hot mixture was filtered and the insoluble part washed with hot ethanol

and filtered again. The combined filtrate was evaporated to give a residue which was submitted to flash chromatography. Elution with $CHCl_3$/MeOH 98/2 afforded desired compounds:

1,4-Bis-(cyanomethyl)piperazine **13a** (71%) ^{1}H NMR ($CDCl_3$): 2.71 (s, 8H); 3.57 (s, 4H); 1,4-bis-(cyanomethyl)-2,6-*cis*-dimethyl piperazine **13b** with (61%) ^{1}H NMR ($CDCl_3$): 1.09 (s, 3H); 1.11 (s, 3H); 1.95 (d, 2H, J = 7.78 Hz); 2.73 (d, 2H J = 7.78 Hz); 2.75–2.77 (m, 2H); 3.50 (s, 2H); 3.77 (s, 2H); 3,8-bis-(cyanomethyl)-3,8-diazabicyclo[3.2.1]octane **13c** (63%) ^{1}H NMR ($CDCl_3$): 1.87–2.02 (m, 4H); 2.58 (dd, 2H, J = 2.19H, 7.78 Hz); 2.73 (d, 2H J = 7.78 Hz); 3.36 (s, 2H); 3.72 (s, 2H); 3.49 (s, 2H).

5.3. General procedure for synthesis of 14a–c

A solution of **13a–c** (500 mg) in THF (20 mL) was added dropwise to a suspension of $LiAlH_4$ (4.6 equiv) in THF (20 mL). The reaction mixture was heated under reflux for 4 h and then cooled in ice, and water (0.47 mL), 15% aqueous NaOH (0.47 mL), and water (1.41 mL) were added sequentially. The resulting granular precipitate was filtered and washed with Et_2O. The combined filtrates were evaporated under reduced pressure, and the residue was chromatographed on silica gel (eluting with MeOH/CH_2Cl_2/NH_4OH, 30:60:10) to give:

1,4-Bis(aminoethyl)piperazine **14a** (87%) ^{1}H NMR ($CDCl_3$): 1.6 (s, 2H); 2.45 (t, 4H, J = 7.45 Hz); 2.51 (br, 8H); 2.81 (t, 4H, J = 7.45 Hz);

1,4-Bis(aminoethyl)-2,6-*cis*-dimethyl piperazine **14b** (73%) ^{1}H NMR ($CDCl_3$): 1.10 (s, 3H); 1.12 (s, 3H); 1.51 (br, 8H); 1.90 (t, 2H, J = 10.12 Hz); 2.40 (t, 2H, J = 7.45 Hz); 2.63–2.82 (m, 10H);

1,4-Bis(aminoethyl)-3,8-diazabicyclo[3.2.1]octane **14c** (53%) ^{1}H NMR ($CDCl_3$): 1.77–1.83 (m, 4H); 2.29 (d, 2H, J = 7.78 Hz); 2.61 (dd, 2H, J = 2.19 H, 7.78 Hz); 3.13 (s, 2H).

5.4. (±)-*trans*-l,2-Cyclopropanedicarboxylic acid (15)

Compound **15** was prepared according to the method of Payne[10] affording crystals, mp 176–177 (lit.[17] mp 177–177.5 °C).

5.5. (±)-*trans*-l,2-Cyclopropanediamine dihydrochloride (16)

Compound **16** was prepared according to the method of Witiak[11] affording diamine dihydrochloride **16** as white crystals, mp 210 °C dec.

5.6. (±)-(*trans*)-*N*,*N*′-Bis[[(*tert*-butoxycarbonyl)amino] propionyl]-ciclopropan-1,2-diamine (17)

A solution of *N*-(*tert*-butoxycarbonyl)-β-alanine (0,1 g, 0,57 mmol) in 5 mL of dichloromethane was treated at 0 °C with 1,1′-carbonyldiimidazole (93 mg, 0,57 mmol). After the mixture was stirred in an ice bath for 1.5 h, **16** (40 mg, 0,28 mmol) in 2 mL of dichloromethane was added and stirred for an additional 1 h at 0 °C. After keeping at room temperature overnight, the solution was washed with a saturated solution of Na_2CO_3 followed by water. This was dried on anhydrous magnesium sulfate and filtered, the solvent was evaporated and the residue was chromatographed on silica gel eluting with CH_2Cl_2/MeOH 95:5 to give **17** (70%).

^{1}H NMR ($CDCl_3$): 1.40 (t, 2H, J = 7.45 Hz); 1.43 (s, 18H); 2.42 (t, 4H, J = 7.02 Hz); 3.03 (t, 2H J = 7.45 Hz); 3.24 (t, 4H, J = 7.02 Hz).

5.7. (±)-(*trans*)-*N*,*N*′-Bis(aminopropionyl)-ciclopropan-1,2-diamine tetrahydrochloride (18)

A solution of **17** (100 mg, 0.26 mmol) in 8 mL of dry methanol, at 0 °C, was saturated with hydrochloric acid (gas). After 1 h at 0 °C, the mixture was stirred at room temperature overnight. The solvent was evaporated, and the residue was washed with diethyl ether and dried, to give the title compound **18** (98%) as a white solid.

^{1}H NMR (D_2O) 1.42 (t, 2H, J = 7.45 Hz); 2.60 (t, 4H, J = 7.02 Hz); 3.04 (t, 2H J = 7.45 Hz); 3.20 (t, 4H, J = 7.02 Hz).

5.8. (±)-(*trans*)-*N*,*N*′-bis(2-aminopropyl)cyclopropane-1,2-diamine tetrahydrochloride (19)

A solution of **18** (450 mg, 1.3 mmol) in 15 mL of anhydrous tetrahydrofuran was added to 28.6 mL of 1 M borane–THF complex solution. This mixture was refluxed for 24 h and cooled to room temperature, and then 20 mL of methanol was added slowly and refluxed for an additional 15 h. After filtration, the solvents were evaporated and the residue dissolved in 5 mL of methanol. After the mixture cooled in an ice bath, 1 mL of concentrated hydrochloric acid was added. This mixture was treated with diethyl ether, and the solid formed was filtered to give the title compound **19** (57%) as a hygroscopic solid.

^{1}H NMR (D_2O): 1.41 (t, 2H, J = 7.45 Hz); 1.63 (m, 4H); 2.67 (m, 8H); 3.05 (t, 2H, J = 7.45 Hz).

5.9. General procedures for synthesis of compounds 5–10

To a suspension of 3-nitro-1,8-naphthalic anhydride (2 equiv) in toluene (5 mL), a solution of corresponding polyamine in ethanol was added drop wise.

The reaction mixture was refluxed for 4 h and then the precipitated solid was filtered and washed with ether and AcOEt to give desired products.

Compound ***5***: Yield (75%): ^{1}H NMR ($CDCl_3$): 3.42 (t, 4H, J = 7.02 Hz); 3.58 (s, 4H); 4.29 (t, 4H, J = 7.02 Hz); 7.93 (t, 2H, J = 7.23 Hz); 8.43 (d, 2H J = 7.23 Hz); 8.73 (d, 2H J = 7.23 Hz); 9.15 (d, 2H J = 2.19 Hz); 9.32 (d, 2H J = 2.19 Hz); ^{13}C (DMSO) as methanesulfonate salt: 38.2, 46.1; 122.8; 123.2; 125.4; 130.1; 130.2; 130.3; 132.4; 135.3; 147.1; 146.4; 164.1; 165.3. MS (ESI) m/z: 597.3. Mp (2 CH_3SO_3H salt) 251.4 °C; Anal. Calcd for $C_{30}H_{24}N_6O_8$: C, 60.40; H, 4.06; N, 14.09; O, 21.46. Found: C, 60.47; H, 4.15; N, 14.22; O, 21.39.

Compound ***6***: (Yield 73%): ^{1}H NMR ($CDCl_3$) 2.64 (s, 8H); 2.74 (t, 4H, J = 6.80 Hz); 4.39 (t, 4H, J = 6.80 Hz); 7.97 (t, 2H, J = 7.23 Hz); 8.44 (d, 2H, J = 7.23 Hz); 8.86 (d, 2H, J = 7.23 Hz); 9.16 (d, 2H, J = 2.19 Hz); 9.34 (d, 2H, J = 2.19 Hz). ^{13}C (DMSO) as methanesulfonate salt: 37.2; 47.2; 50.7; 55.2; 122.7; 123.2; 124.7; 130.1; 130.2; 130.3; 131.3; 134.9; 137.4; 146.2; 164.4; 165.2. MS (ESI) m/z: 622.7. Mp (2 CH_3SO_3H salt) 298 °C dec. Anal. Calcd for $C_{32}H_{26}N_6O_8$: C, 61.73; H, 4.21; N, 13.50; O, 20.56. Found: C, 61.69; H, 4.12; N, 14.72; O, 20.60.

Compound ***7***: (Yield 82%): ^{1}H NMR ($CDCl_3$) 1.34 (s, 3H); 1.36 (s, 3H); 2.03 (t, 2H, J = 9.87 Hz); 2.70 (t, 2H, J = 7.13 Hz); 2.76–2.88 (m, 2H); 2.92–3.05 (m, 4H); 4.24–4.34 (m, 2H); 4.38 (t, 2H, J = 7.13 Hz); 7.97 (t, 2H, J = 7.23 Hz); 8.44 (d, 2H J = 7.23 Hz); 8.86 (d, 2H, J = 7.23 Hz); 9.16 (d, 2H, J = 2.19 Hz); 9.34 (d, 2H, J = 2.19 Hz). ^{13}C (DMSO) as methanesulfonate salt: 14.3; 37.2; 46.2; 50.1; 55.2; 59.3; 64.6; 122.8; 123.2; 125.4; 126.8, 130.1; 130.2; 130.3; 132.3; 132.4; 135.4; 137.1; 146.3; 164.2; 165.3. MS (ESI) m/z: 651.3. Mp (2 CH_3SO_3H salt) 233.0 °C. Anal. Calcd for $C_{34}H_{30}N_6O_8$: C, 62.76; H, 4.65; N, 12.92; O, 19.67. Found: C, 62.82; H, 4.79; N, 13.09; O, 19.59.

Compound ***8***: (Yield 83%): ^{1}H NMR ($CDCl_3$) 2.31 (d, 2H, J = 9.98 Hz); 2.61–2.67 (m, 8H); 2.72 (d, 2H, J = 9.98 Hz); 3.23 (s, 2H); 4.28–4.34 (m, 4H); 7.91 (t, 2H, J = 7.13 Hz); 8.34 (d, 2H, J = 7.13 Hz); 8.78 (d, 2H, J = 7.13 Hz); 9.14 (d, 2H, J = 2.19 Hz); 9.32 (d, 2H, J = 2.19 Hz).

^{13}C (DMSO) as methanesulfonate salt: 22.2; 25.1; 37.2; 50.1; 55.2; 59.3; 60.1; 122.8; 123.2; 125.4; 126.8, 130.1; 130.2; 130.3;

132.3; 132.4; 135.4; 137.1; 146.3; 164.2; 165.3.MS (ESI) *m*/*z*: 648.95. Mp (2 CH_3SO_3H salt) 252.8 °C. Anal. Calcd for $C_{34}H_{28}N_6O_8$: C, 62.96; H, 4.35; N, 12.96; O, 19.73. Found: C, 62.84; H, 4.73; N, 13.10; O, 19.55.

Compound ***9***: Yield (75%): ^{1}H NMR ($CDCl_3$): 1.96 (m, 4H); 2.67 (t, 8H, *J* = 7.02 Hz); 4.31 (t, 2H, *J* = 7.02 Hz);7.97 (t, 2H *J* = 7.23 Hz); 8.44 (d, 2H, *J* = 7.23 Hz); 8.80 (d, 2H *J* = 7.23 Hz); 9.15 (d, 2H, *J* = 2.19 Hz); 9.32 (d, 2H, *J* = 2.19 Hz). ^{13}C (DMSO) as methanesulfonate salt: 24.3; 37.2; 38.2, 46.1; 122.8; 123.2; 125.4; 130.1; 130.2; 130.3; 132.4; 135.3; 137.1; 146.4; 164.1; 165.3. MS (ESI) *m*/*z*: 625.3. Mp (2 CH_3SO_3H salt) 223.0 °C. Anal. Calcd for $C_{32}H_{28}N_6O_8$: C, 61.53; H, 4.52; N, 13.46; O, 20.49. Found: C, 61.44; H, 4.39; N, 13.29; O, 20.55.

Compound ***10***: (Yield 68%): ^{1}H NMR ($CDCl_3$): 1.42 (t, 2H *J* = 7.45 Hz); 1.80 (m, 4H); 2.15 (t, 4H, *J* = 7.02 Hz); 3.05 (t, 2H, *J* = 7.45 Hz); 4.31 (t, 4H, *J* = 7.02 Hz); 7.97 (t, 2H, *J* = 7.23 Hz); 8.44 (d, 2H, *J* = 7.23 Hz); 8.80 (d, 2H, *J* = 7.23 Hz); 9.15 (d, 2H, *J* = 2.19 Hz); 9.32 (d, 2H, *J* = 2.19 Hz). ^{13}C (DMSO) as methanesulfonate salt: 15.5; 28.3; 35.9; 37.2; 37.9; 42.5; 122.6; 123.1; 124.5; 130.1; 130.2; 130.3; 131.3; 134.9; 137.4; 146.2; 164.4; 165.2 MS (ESI) *m*/*z*: 636.72. Mp (2 CH_3SO_3H salt) 243.8 °C. Anal. Calcd for $C_{33}H_{28}N_6O_8$: C, 62.26; H, 4.43; N, 13.20; O, 20.11. Found:, 62.22; H, 4.55; N, 13.09; O, 20.07.

5.10. Naphthalimidobutanol (21a)

A mixture 1,8-napthalic anhydride (2.5 g, 0.013 mol), and 4-amino-1-butanol (3.6 mL, 0.04 mmol) in water (10 mL) was refluxed for 30 min and then cooled at 4 °C. Then product 7a formed was filtered, washed with ice cold water and crude product was recrystallized from acetone and dried over P_2O_5 to give the compound **21a** as white crystalline solid (89%).

^{1}H NMR ($CDCl_3$) 1.65–1.95 (m, 4H); 3.75 (t, 2H, *J* = 5.92 Hz); 4.25 (t, 2H, *J* = 7.45 Hz); 7.75 (t, 2H, *J* = 7.67 Hz); 8.20 (d, 2H, *J* = 8.11 Hz); 8.6 (d, 2H, *J* = 7.13 Hz).

5.11. 3-Nitro-naphthalimidobutanol (21b)

Compound **21b** was prepared using 3-nitro-1,8-naphthalic anhydride following the above-described procedure.

Yield 86%. ^{1}H NMR ($CDCl_3$) 1.65–1.95 (m, 4H); 3.75 (t, 2H, *J* = 6.40 Hz); 4.30 (t, 2H, *J* = 7.45 Hz); 7.95 (t, 1H, *J* = 7.78 Hz); 8.45 (d, 1H, *J* = 8.33 Hz); 8.8 (d, 1H, *J* = 7.23 Hz); 9.15 (d, 1H, *J* = 2.19 Hz); 9.35 (d, 1H, *J* = 2.19 Hz).

5.12. O-tosylbutyloxynaphthalimide (22a)

Naphthalimidobutanol (**21a**) (1.0 g, 3.7 mmol) was dissolved in anhydrous CH_2Cl_2 (10 mL) followed by the addition of tosyl chloride (2.89 g, 14.85 mmol) and triethylamine (2.8 mL, 20.4 mmol). The solution was left overnight at 50 °C. After cooling the CH_2Cl_2 solution was washed with water and saturated bicarbonate solution. After drying and the removal of the solvent, a dark residue was obtained which was then recrystallized from hot ethanol as a white powder (55%).

^{1}H NMR ($CDCl_3$) 1.60–1.80 (m, 4H); 2.40 (s, 3H); 4.10 (br, 2H); 4.20 (br, 2H); 7.34 (d, 2H, *J* = 8.00 Hz); 7.70–7.90 (m, 4H); 8.25 (d, 2H, J = 8.22 Hz); 8.6 (d, 2H, J = 7.23 Hz).

5.13. *O*-Tosylbutyloxy-3-nitronaphthalimide (22b)

Compound **22b** was prepared following the above described procedure starting from **21b**. Yellow powder, yield 46%. ^{1}H NMR ($CDCl_3$) 1.70–1.85 (m, 4H); 2.50 (s, 3H); 4.10 (br, 2H); 4.20 (br, 2H); 7.35 (d, 2H, *J* = 8.00 Hz); 7.80 (d, 2H, *J* = 8.00 Hz); 8.00 (t, 1H, *J* = 7.78 Hz); 8.55 (d, 1H, *J* = 8.33 Hz); 8.80 (d, 1H, *J* = 7.23 Hz); 9.15 (d, 1H, *J* = 2.19 Hz); 9.35 (d, 1H, *J* = 2.19 Hz).

5.14. N^1,N^3,N^7,N^{10}-tetramesytil-1,3-bis(2-aminoethyl)-1,3-propanediamine (23)

N,*N*′-Bis(2-aminoethyl)-1,3propanediamine (1.0 g, 6.05 mmol) was dissolved in anhydrous pyridine (22 mL) followed by the addition of mesitylene chloride (5.4 g, 24.8 mmol). The resulting solution was stirred at room temperature for 4 h. Pyridine was evaporated and the crude product was recrystallized from hot ethanol as a yellow powder (59%).

^{1}H NMR ($CDCl_3$): 1.75–1.90 (m, 2H); 2.35 (s, 12H); 2.55 (s, 12H); 2.60 (s, 12H); 2.95 (q, 4H, *J* = 6.14 Hz); 3.15 (t, 4H, *J* = 7.23 Hz); 3.35 (t, 4H, *J* = 6.14 Hz); 6.90 (s, 8H).

5.15. General procedures for N-alkylation reaction (24a–b)

N^1,N^3,N^7,N^{10}-Tetramesytil-1,3-bis(2-aminoethyl)-1,3-propanediamine (**23**) (0.651 mmol) was dissolved in anhydrous DMF (13.5 mL) followed by the addition of **22a–b** (0.13 mmol) and caesium carbonate (1.06 g). The solution was left at 80 °C. Completion of the reaction was monitored by thin-layer chromatography. DMF was removed under vacuo, and the residue was poured into cold water and the resulted precipitate filtered and washed thoroughly with water. After drying, the crude product was recrystallised from ethanol to give the fully protected pure product in high yield.

Compound ***24a***. (Yield 85%) ^{1}H NMR ($CDCl_3$): 1.30–1.70 (m, 10H); 2.15 (s, 12H); 2.35 (s, 12H); 2.60 (s, 12H); 2.55 (s, 12H); 2.95 (q, 4H, *J* = 6.14 Hz); 3.15 (t, 4H, *J* = 6.14 Hz); 3.25 (s, 8H); 4.00 (t, 4H, *J* = 7.45 Hz); 6.88 (s, 4H); 7.02 (s, 4H); 7.75 (t, 4H, *J* = 7.78 Hz); 8.25 (d, 4H, *J* = 7.78 Hz); 8.60 (d, 4H, *J* = 7.78 Hz).

Compound ***24b***. (Yield 95%) ^{1}H NMR ($CDCl_3$): 1.30–1.70 (m, 10H); 2.15 (s, 12H); 2.35 (s, 12H); 2.60 (s, 12H); 2.55 (s, 12H); 2.95 (q, 4H, *J* = 6.14 Hz); 3.15 (t, 4H, *J* = 6.14 Hz); 3.25 (s, 8H); 4.00 (t, 4H, *J* = 7.45 Hz); 6.88 (s, 4H); 7.02 (s, 4H); 8.00 (t, 2H, *J* = 7.78 Hz); 8.55 (d, 2H, *J* = 8.33 Hz); 8.80 (d, 2H, *J* = 7.23 Hz); 9.15 (d, 2H, *J* = 2.19 Hz); 9.35 (d, 2H, *J* = 2.19 Hz).

5.16. General procedures for deprotection reaction (11–12)

The fully protected polyamine derivatives (**24a–b**) (0.222 mmol) were dissolved in anhydrous dichloromethane (10 mL) followed by the addition of hydrobromic acid/glacial acetic acid (1 mL). The solution was left stirring at room temperature for 24 h. The yellow precipitate formed was filtered off and washed with dichloromethane, ethyl acetate and ether.

Compound ***11***. (Yield 97%) ^{1}H NMR (D_2O) 1.50–1.90 (m, 8H); 2.15–2.28 (m, 2H); 3.15–3.32 (m, 8H); 3.56 (br, 8H); 3.9 (t, 4H, *J* = 7.45 Hz) 7.05 (t, 4H, *J* = 7.78 Hz); 7.90 (d, 4H, *J* = 7.78 Hz); 8.15 (d, 4H, *J* = 7.78 Hz). ^{1}H NMR (DMSO): 23.3; 24.2; 25.6; 43.3; 43.4; 45.0; 47.7; 122.8; 128.2; 131.7; 132.2; 135.3; 164.4. MS (ESI) *m*/*z*: 633.43. Mp (4 HBr salt) 235.6 °C Anal. Calcd for $C_{38}H_{44}N_6O_4$: C, 70.35; H, 6.84; N, 12.95; O, 9.86. Found: C, 70.30; H, 6.72; N, 12.80; O, 9.80.

Compound **12**. (Yield 93%) ^{1}H NMR (D_2O) 1.50–1.90 (m, 8H); 2.15–2.28 (m, 2H); 3.15–3.32 (m, 8H); 3.56 (br, 8H); 3.9 (t, 4H, *J* = 7.45 Hz); 8.07 (t, 2H, *J* = 7.78 Hz); 8.57 (d, 2H, *J* = 8.33 Hz); 8.73 (d, 2H, *J* = 7.23 Hz); 9.18 (d, 2H, *J* = 2.19 Hz); 9.24 (d, 2H, *J* = 2.19 Hz). ^{1}H NMR (DMSO): 23.2; 24.4; 25.3; 43.3; 43.5; 45.2; 47.7; 122.8; 123.2; 125.4; 130.1; 130.2; 130.3; 132.4; 135.3; 147.1; 146.4; 164.1; 165.3. MS (ESI) *m*/*z*: 753.45. Mp (4 HBr salt) 244.6 °C Anal. Calcd for $C_{34}H_{42}N_8O_8$: C, 61.78; H, 5.73; N, 15.17; O, 17.33. Found: C, 61.70; H, 5.60; N, 15.03; O, 17.39.

5.17. Biological tests

5.17.1. Cells culture

Human colon adenocarcinoma HT-29 cells were cultured in DMEM supplemented with 2 mM L-glutammine, 10% heat-inacti-

vated foetal bovine serum (FBS), 1% penicillin/streptomycin (all from Cambrex Bioscience, Verviers, Belgium) at 37 °C in an atmosphere of 95% O_2 and 5% CO_2. The cells were plated at density of 5×10^5 in 6-cm cell culture dishes the day before treatment with compounds **9** and **10** at different concentrations. Z-VAD-FMK (50 μM) (BD Bioscience, USA) was administrated to cells 30 min before compounds analysed. At the end of the incubation times cells were processed for detection of apoptosis by FACS analysis.

5.17.2. MTT assay

HT-29 cells (1×10^5 cells/ml in 96-well culture plates) were incubated for 72 h with different concentrations of compounds (**5–12**) dissolved in DMSO. After treatment, MTT solution (5 mg/ml in PBS) was added to each well. After 3 h incubation lysis buffer (200 g/L SDS, 50% Formamide, pH 4.7) was added to each well to dissolve formazan. The absorbance was measured at 620 nm with a Microplate reader. All experiments were performed at least three times and average of the percentage absorbance was plotted against concentration. The results were expressed as percentage relative to untreated control and IC_{50} value was calculated for each compounds.

5.17.3. Analysis of apoptosis

Hypodiploid DNA was analysed using propidium iodide staining (PI) by flow cytometry as described.[18] Briefly, cells were washed in phosphate buffered saline (PBS) and resuspended in 500 μl of a solution containing 0.1% sodium citrate, 0.1% Triton X-100 and 50 μg/ml PI (Sigma–Aldrich). After incubation at 4 °C for 30 min in the dark, cell nuclei were analysed with Becton Dickinson FACScan flow cytometer using CellQuest program. Cellular debris was excluded from analysis by raising the forward scatter threshold, and the DNA content of the nuclei was registered on a logarithmic scale. The percentage of cells in the hypodiploid region was calculated.

5.17.4. Statistical analysis

All results are shown as means ± SEM of three experiments performed in triplicate. Statistical comparison between groups were made using parametric Bonferroni test. *P* values <0.05 were considered significant.

5.17.5. DNA cleavage assays

DNA cleavage reactions were performed with recombinant human DNA topo IIα, purified as described.[19] pBR322 plasmid (5 ng) was incubated with equal amounts of the enzyme in the presence of different drug concentrations in 10 mM Tris–Cl, pH 7.5, 150 mM KCl, 5 mM EDTA, 10 mM $MgCl_2$, 0.01 mg/mL BSA, 10 mM DTT and 1 mM ATP. The reactions were incubated for 30 min at 37 °C, and then stopped with 0.1% SDS and 0.5 mg/mL proteinase K (Sigma) for 30 min at 45 °C. DNA samples were then run in 1% agarose gels containing 0.05% SDS, and after extensive washing the gel was stained with ethidium bromide. Then, DNA fragments were transferred to nitrocellulose membranes and blocked with UV irradiation. pBR322 DNA was labelled with ^{32}P-dCTP with Ready-to-go DNA labelling Kit (GE Healthcare) and used as a probe to hybridize the DNA fragments onto the membrane. Hybridization reaction was performed in 0.5 M Na-phosphate, pH 7.2, 1 mM EDTA, 7% SDS and 1% BSA at 65 °C. After final washes in 1x SSC and 0.1% SDS at 65 °C, membranes were exposed for 1–24 h, and images were then acquired with a Molecular Dynamics PhosphorImager.

5.17.6. Computational details

Autodock 3.0.5[10] is used for all docking calculations. The NMR structure of the covalent complex between d(CGCTAGGCG)-(GCGATCCGC) and the bis-thiazole orange (PDB archive code 108D), is used as a template to build the homology Model A deleting the ligand structure (Macromodel 8.5 Software Package).[20] From Model A we have built the Model B changing the T4 and T12, A5 and A13 in C and G residues, respectively. The same steps are made for the Model C using as template the X-ray structure 367D (PDB archive code). We have eliminated the ligands and water molecules, and converted the Br-U3 and Br-U9 in T residues.

The **3** and **5–12** geometries are optimized at the hybrid DFT B3LYP level using the 6-31G(d) basis set (Gaussian 03 Software Package).[21] Torsion restraints have been employed to avoid the formation of intramolecular hydrogen bonds affecting the atomic charge values. Subsequently, the charges of **3** and **5–12** are calculated by the ChelpG method[21] at the B3LYP/6-31 + G(d) level. The above calculated charges are used for the docking calculations.

For all the docking calculations of **3** and **5–10**, a grid box size of $52 \times 52 \times 60$ with spacing of 0.375 Å between the grid points, centred between central base pairs and covering the minor and major groove surface of DNA is used. The same criteria are used for all the docking calculations of **11** and **12**, but through a grid box size of $58 \times 68 \times 58$.

In order to achieve a representative conformational space during the docking calculations on **3** and **5–10**, seven calculations consisting of 256 runs are performed, obtaining 1792 structures (256×7). The Lamarkian genetic algorithm is used for dockings. An initial population of 150 randomly placed individuals, a maximum number of 2.5×10^5 energy evaluations, and a maximum number of 2.7×10^4 generations are taken into account. A mutation rate of 0.02, a crossover rate of 0.8 and local search frequency of 0.06 are used.

The docking calculation parameters on **11** and **12** are incremented for the larger number of active torsions. An initial population of 600 randomly placed individuals, a maximum number of 5×10^6 energy evaluations, and a maximum number of 6×10^6 generations are taken into account. A mutation rate of 0.02, a crossover rate of 0.8 and local search frequency of 0.26 are used.

Results (**3** and **5–12**) differing by less than 2 Å in positional root-mean-square deviation (RMSD) are clustered together and represented by the result with the most favourable free energy of binding.

All the 3D models are depicted using the Phyton software:[22] molecular surfaces are rendered using Maximal Speed Molecular Surface (MSMS).[23]

Acknowledgment

Giovanni Capranico acknowledges financial support from Associazione Italiana per la Ricerca sul Cancro (AIRC), Milan, Italy.

References and notes

1. Braña, M. F.; Ramos, A. *Curr. Med. Chem. Anticancer Agents* **2001**, *1*, 237.
2. Nitiss, J. L.; Zhou, J.; Rose, A.; Hsiung, Y.; Gale, K. C.; Osheroff, N. *Biochemistry* **1998**, *37*, 3078.
3. Malviya, V. K.; Liu, P. Y.; Alberts, D. S.; Surwit, E. A.; Craig, J. B.; Hanningan, E. V. *Am. J. Clin. Oncol.* **1992**, *15*, 41.
4. Bousquet, P. F.; Braña, M. F.; Conlon, D.; Fitzgerald, K. M.; Perron, D.; Cocchiaro, C.; Miller, R.; Moran, M.; George, J.; Qian, X.-D.; Keilhauer, G.; Romerdahl, C. *Cancer Res.* **1995**, *55*, 1176.
5. Bailly, C.; Braña, M. F.; Waring, J. *Eur. J. Biochem.* **1996**, *240*, 195.
6. Gamage, S. A.; Spicer, J. A.; Finlay, G. J.; Stewart, A. J.; Charlton, P.; Baguley, B. C.; Denny, W. A. *J. Med. Chem.* **2001**, *44*, 1407.
7. Cholody, W. C.; Kosakowska-Cholody, T.; Hollingshead, M. G.; Hariprakasha, H. K.; Michejda, C. J. *J. Med. Chem.* **2005**, *48*, 4474.
8. Holden, J. A. *Curr. Med. Chem. Anticancer Agents* **2001**, *1*, 1.
9. Filosa, R.; Peduto, A.; de Caprariis, P.; Festa, M.; Petrella, A.; Pau, A.; Pinna, G. A.; La Colla, P.; Busonera, B.; Loddo, R. *Eur. J. Med. Chem.* **2007**, *42*, 293.
10. Payne, G. B. *J. Org. Chem.* **1967**, *32*, 3351.
11. Witiak, D. T.; Lee, H. J.; Hart, R. W.; Gibson, R. E. *J. Med. Chem.* **1977**, *20*, 630.
12. Capranico, G.; Binaschi, M.; Borgnetto, M. E.; Zunino, F.; Palumbo, M. *Trends Pharmacol. Sci.* **1997**, *18*, 323.
13. Morris, G. M.; Goodsell, D. S.; Halliday, R. S.; Huey, R.; Hart, W. E.; Belew, R. K.; Olson, A. J. *J. Comp. Chem.* **1998**, *19*, 1639.

14. Breneman, C. M.; Wiberg, K. B. *J. Comp. Chem.* **1990**, *11*, 361.
15. Oliveira, J.; Ralton, L.; Tavares, J.; Codeiro-da-Silva, A.; Bestwick, C. S.; McPherson, A.; Lin, P. K. T. *Bioorg. Med. Chem. Lett.* **2007**, *10*, 541.
16. Lin, P. K. T.; Pavlov, V. A. *Bioorg. Med. Chem. Lett.* **2000**, *10*, 1609.
17. McCoy, L. L. *J. Am. Chem. Soc.* **1958**, *80*, 6568.
18. Nicoletti, I.; Migliorati, G.; Pagliacci, M. C.; Grignani, F.; Riccardi, C. *J. Immunol. Methods* **1991**, *139*, 271.
19. Guano, F.; Pourquier, P.; Tinelli, S.; Binaschi, M.; Bigioni, M.; Animati, F.; Manzini, S.; Zunino, F.; Kohlhagen, G.; Pommier, Y.; Capranico, G. *Mol. Pharmacol.* **1999**, *56*, 77.
20. MacroModel, version 8.5, Schrödinger LLC, New York, NY, 2003.
21. Frisch, M. J.; Trucks, G. W.; Schlegel, H. B.; Scuseria, G. E.; Robb, M. A.; Cheeseman, J. R.; Montgomery J. A.; Jr, Vreven, T.; Kudin, K. N.; Burant, J. C.; Millam, J. M.; Iyengar, S. S.; Tomasi, J.; Barone, V.; Mennucci, B.; Cossi, M.; Scalmani, G.; Rega, N.; Petersson, G. A.; Nakatsuji, H. Hada, M.; Ehara, M.; Toyota, K.; Fukuda, R.; Hasegawa, J.; Ishida, M.; Nakajima, T.; Honda, Y.; Kitao, O.; Nakai, H.; Klene, M.; Li, X.; Knox, J. E.; Hratchian, H. P.; Cross, J. B.; Adamo, C.; Jaramillo, J.; Gomperts, R.; Stratmann, R. E.; Yazyev, O.; Austin, A. J.; Cammi, R.; Pomelli, C.; Ochterski, J. W.; Ayala, P. Y.; Morokuma, K.; Voth, G. A.; Salvador, P.; Dannenberg, J. J.; Zakrzewski, V. G.; Dapprich, S.; Daniels, A. D.; Strain, M. C.; Farkas, O.; Malick, D. K.; Rabuck, A. D.; Raghavachari, K.; Foresman, J. B.; Ortiz, J. V.; Cui, Q.; Baboul, A. G.; Clifford, S.; Cioslowski, J.; Stefanov, B. B.; Liu, G.; Liashenko, A.; Piskorz, P.; Komaromi, I.; Martin, R. L.; Fox, D. J.; Keith, T.; Al-Laham, M. A.; Peng, C. Y.; Nanayakkara, A.; Challacombe, M.; Gill, P. M. W.; Johnson, B.; Chen, W.; Wong, M. W.; Gonzalez, C.; Pople, J. A. Gaussian 03, revision B.05, Gaussian, Inc., Pittsburgh, PA, 2003.
22. Sanner, M. F. *J. Mol. Graph. Model.* **1999**, *17*, 57–61.
23. Sanner, M. F.; Olson, A. J.; Spehner, J. C. *Biopolymers* **1996**, *38*, 305–320.